

Journal of Mechanics of Materials and Structures

**TOPOLOGY OPTIMIZATION OF GEOMETRICALLY NONLINEAR
STRUCTURES TRACING GIVEN LOAD-DISPLACEMENT CURVES**

Gil Ho Yoon, Jin Yee Noh and Yoon Young Kim

Volume 6, No. 1-4

January–June 2011

TOPOLOGY OPTIMIZATION OF GEOMETRICALLY NONLINEAR STRUCTURES TRACING GIVEN LOAD-DISPLACEMENT CURVES

GIL HO YOON, JIN YEE NOH AND YOON YOUNG KIM

To design structures involving nonlinear structural responses by the topology optimization method is still a challenging problem. Here, the structural topology optimization tracing nonlinear load-displacement curves is investigated by employing the element connectivity parametrization formulation as it is expected to deal with low-density element related numerical instability more effectively than the element density based formulation. After the formulation is given in the setting of the element connectivity parametrization, the sensitivity analysis for load-displacement curve tracing problems implemented with a discretized finite element model is presented. Several numerical problems are considered to address issues occurring in the topology optimization of nonlinear structures. Finally, the findings from this investigation on the topology optimization tracing nonlinear load-displacement trajectories and future work are summarized as concluding remarks.

1. Introduction

Along with size and shape optimization methods, the topology optimization method [Bendsøe and Kikuchi 1988] has been used as an effective tool for optimizing structures and mechanical parts (see [Bendsøe and Sigmund 2003], for example). Compared with abundant investigations on linear structural problems, the topology optimization of nonlinear structural problems is relatively rare [Buhl et al. 2000; Bruns et al. 2002; Cho and Jung 2003; Yoon and Kim 2005b; Yoon et al. 2008]. In this study, we investigate the topology optimization of a continuum structure tracing a prescribed nonlinear load-displacement trajectory. Specifically, hardening or softening nonlinear responses without and without snap-through will be considered.

Structures exhibiting geometric hardening or softening behavior (see Figure 1) can be utilized for crash worthiness or energy absorption mechanism design. For example, one may wish to find a structure which can absorb a specific amount of impact energy in case of crash worthiness. There have been some interests in designing truss or beam structures to exhibit geometrical and/or material nonlinearities [Kamat and Ruangsilasingha 1985; Saxena 2005; Lu and Kota 2003; Ohsaki 2005; Huang and Xie 2008; Santer and Pellegrino 2008; Thai and Kim 2009] where the buckling loads of structures are maximized.

This research was supported by the National Creative Research Initiatives Program (Korea Research Foundation No. 2009-0083278) contracted through the Institute of Advanced Machinery and Design at Seoul National University, by the WCU (World Class University) program (Grant No. R31-2008-000-10083-0) through the Korea Research Foundation funded by the Ministry of Education, Science, and Technology and by the Regional Core Research Program/Anti-aging and Well-being Research Center funded by the Grant of the Korean Ministry of Education, Science and Technology.

Keywords: topology optimization, element connectivity parametrization method, hardening or softening load-displacement trajectory.

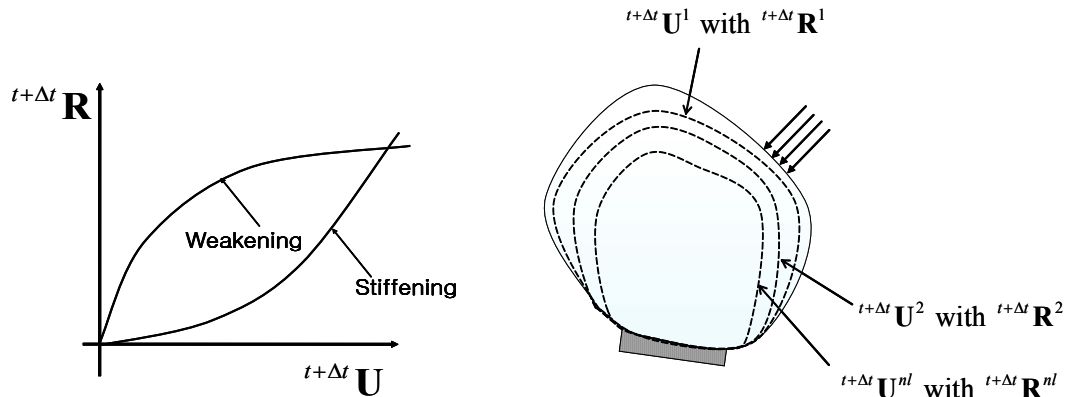


Figure 1. Geometric hardening or weakening model depicted with a displacement controlled Newton–Raphson scheme. (The prescribed displacement and the reaction force of the i -th load step are denoted by $t+\Delta t \mathbf{U}^i$ and $t+\Delta t \mathbf{R}^i$, respectively. The number of load steps is nl).

However, research on two- or three-dimensional continuum structures is relatively less active due to heavy computational cost and numerical instability [Buhl et al. 2000; Bruns et al. 2002; Yoon et al. 2007].

Perhaps, the first investigation on trajectory-following continuum topology optimization was done in [Sekimoto and Noguchi 2001] using the homogenization method. Trajectory problems were also solved in [Bruns et al. 2002] and [Bruns and Sigmund 2004] using the density based method. In these studies, an automated solution controlling method was employed to consider a snap-through phenomenon. To design compliant mechanisms generating given paths was also considered using the structural topology optimization algorithms [Lu and Kota 2003; Saxena 2005; Prasad and Diaz 2006]. In spite of these studies, some issues, such as low-density elements, still remain. Among others, this study is focused on the numerical instability of low-density elements and the adverse effects of postprocessing intermediate density elements to solid or void elements.

An optimized layout even at the converged state typically involves some low-density (and intermediate-density) elements. In this case, low-density continuum elements under a big load can inevitably lose the positive-definiteness of the system tangent stiffness matrix when nonlinear analysis is performed. Among others, Yoon and Kim [2005b] developed a method, called the element connectivity parametrization method (ECP) to avoid the loss of the positive definiteness of the system matrix. The concept of the ECP method may be briefly illustrated with Figure 2; see [Yoon and Kim 2005a; [2005b]; Langelaar et al. 2005; Yoon et al. 2007; 2008; Yoon 2010] for more details. In the ECP method, elements are connected through one-dimensional zero-length links having variable stiffness. Because the ECP method represents an element of low density by a solid element connected through one-dimensional low-stiffness links, the loss of the tangent stiffness of low-density continuum elements can be avoided. To avoid the aforementioned numerical instability, therefore, we will employ the ECP method for the present problem tracing a geometrically nonlinear load-displacement curve.

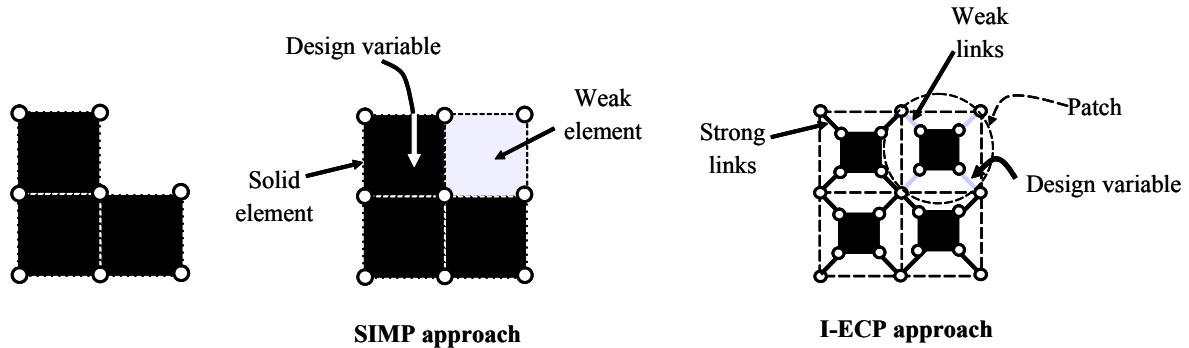


Figure 2. A structure (left) modeled with the SIMP (solid isotropic with penalization) method (middle) and the ECP-based method (right). All links have zero length.

Another important issue, especially in problems involving nonlinear structural responses, is related to intermediate-density elements appearing at the converged state because the postprocessing of intermediate elements to either solid or void elements can produce considerably different load-displacement curves. Although an implicit (and/or explicit) penalization technique to push discretizing elements to either void or solid states can be used, any topology optimization formulation using the notion of the density concept cannot completely suppress intermediate density-elements at the convergence state. (Integer-type topology optimization is not considered here because of impractically high computation cost.) For this reason, a special attention will be paid to the issue related to intermediate densities.

For the numerical analysis of geometrically nonlinear structures here, the displacement-controlled Newton–Raphson method will be used [Bathe 1996; Cho and Jung 2003; Huang and Xie 2008]. If a force control procedure is implemented, it is difficult to simulate complicated load-displacement trajectories such as snap-through or snap-back phenomena [Bathe 1996; Sekimoto and Noguchi 2001; Huang and Xie 2008]. Alternatively, one can use algorithms such as the arc-length method or the Broyden–Fletcher–Goldfarb–Shanno (BFGS) method (see [Bathe 1996], for example) when snap-back or snap-through phenomena need to be simulated. Since a monotonic softening or hardening load-displacement trajectory and a simple snap-through example are of the main interests in this study, the displacement-controlled Newton–Raphson method would be satisfactory here.

This paper is organized as follows. Section 2 explains the underlying governing equations for non-linear analysis and the concept of the ECP modeling and Section 3 presents the topology optimization formulation and sensitivities analyses needed to solve load-displacement tracing problems. In Section 4, several numerical case studies are presented. Finally, the findings of this research are summarized and future research work is discussed.

2. Underlying equations and the ECP method

Before presenting an optimization formulation, this section describes underlying equations and notations needed for the finite element analysis and the ECP formulation.

2.1. Geometrical nonlinear analysis. For the analysis of geometrical nonlinear structures, the following Green–Lagrangian strain (${}^{t+\Delta t}_0 \varepsilon_{ij}$) and the associated second PK (Piola–Kirchhoff) stress are used:

$${}^{t+\Delta t}_0 \varepsilon_{ij} = \frac{1}{2} \left({}^{t+\Delta t}_0 u_{i,j} + {}^{t+\Delta t}_0 u_{j,i} + {}^{t+\Delta t}_0 u_{l,i} {}^{t+\Delta t}_0 u_{l,j} \right) \quad (i = 1, 2), \quad (1)$$

where ${}^{t+\Delta t}_0 u_i$ is the displacement component in the x_i coordinate at time $t + \Delta t$ where the left subscript 0 indicates that the displacement is measured in the undeformed configuration. The comma denotes partial differentiation with respect to coordinate x_i . The repeated index implies summation. By denoting the displacement increment nodal vector and the displacement nodal vector at time $t + \Delta t$ of a generic point of a body occupying a domain V in equilibrium by $\Delta \mathbf{U}$ and ${}^{t+\Delta t} \mathbf{U}$, respectively, the following update rules for the Newton–Raphson method can be used (see [Bathe 1996; Cook et al. 2001], for instance):

$$\mathfrak{R} = {}^{t+\Delta t} \mathbf{F}_{\text{Ext}} - {}^{t+\Delta t} \mathbf{F}_{\text{Int}} = {}^{t+\Delta t} \mathbf{F}_{\text{Ext}} - \int_V \mathbf{B}^T \mathbf{S} dV = \mathbf{0} \quad (\mathbf{S} = \mathbf{C} \mathbf{E}), \quad (2)$$

$${}^t \mathbf{K}_T = \frac{\partial \mathfrak{R}}{\partial {}^{t+\Delta t} \mathbf{U}}, \quad (3)$$

$${}^{t+\Delta t} \mathbf{U}^{(k)} = {}^{t+\Delta t} \mathbf{U}^{(k-1)} + \Delta \mathbf{U}^{(k)}, \quad {}^{t+\Delta t} \mathbf{U}^{(0)} = {}^t \mathbf{U}, \quad (4)$$

$${}^t \mathbf{K}_T^{(k-1)} \Delta \mathbf{U}^{(k)} = \mathfrak{R}({}^{t+\Delta t} \mathbf{U}^{(k-1)}), \quad (5)$$

where superscript k denotes the iteration step in the implemented Newton–Raphson method. The residual vector and the tangent stiffness matrix are denoted by \mathfrak{R} and ${}^t \mathbf{K}_T$, respectively. The symbols ${}^{t+\Delta t} \mathbf{F}_{\text{Ext}}$ and ${}^{t+\Delta t} \mathbf{F}_{\text{Int}}$ denote the external load and internal load, respectively. The vector expressions of the second PK stress and the Green-strain are given by \mathbf{S} and \mathbf{E} and they are assumed to be related through a linear constitutive matrix \mathbf{C} . The strain-displacement matrix is denoted by \mathbf{B} .

2.2. Geometrical nonlinear analysis for the ECP method. In representing a layout in the framework of the ECP method, elements are not directly connected but through one-dimensional zero-length links with varying stiffness values. Therefore, the total number of nodes by ECP for two- or three-dimensional problems can be increased approximately by 5 or 9 times compared to those by the standard density approach [Yoon et al. 2007]. However, one can reduce the computation time and the size of the assembled system matrix by employing the patch model of [Yoon 2010; Yoon et al. 2007] (Figure 3) and using static condensation. Referring to Figure 3, the degrees of freedom of the inner nodes of the ECP patch can be statically condensed out so that only the degrees of freedom of the outer nodes can be kept in the system matrix. (For sample code in Matlab of the patch-model based ECP method, see [Yoon et al. 2008]).

Although only the degrees of freedom of the outer nodes will appear in the final system matrix, the displacement $\mathbf{u}_{e,\text{in}}^{(k)}$ of the inner nodes and the displacement $\mathbf{u}_{e,\text{out}}^{(k)}$ of the outer nodes should be simultaneously updated as

$$\begin{bmatrix} {}^{t+\Delta t} \mathbf{u}_{e,\text{out}}^{(k)} \\ {}^{t+\Delta t} \mathbf{u}_{e,\text{in}}^{(k)} \end{bmatrix} = \begin{bmatrix} {}^{t+\Delta t} \mathbf{u}_{e,\text{out}}^{(k-1)} \\ {}^{t+\Delta t} \mathbf{u}_{e,\text{in}}^{(k-1)} \end{bmatrix} + \begin{bmatrix} \Delta \mathbf{u}_{e,\text{out}}^{(k)} \\ \Delta \mathbf{u}_{e,\text{in}}^{(k)} \end{bmatrix} \quad (6)$$

The updated displacement increments for the outer nodes and the inner nodes are denoted by $\Delta \mathbf{u}_{e,\text{out}}^{(k)}$ and $\Delta \mathbf{u}_{e,\text{in}}^{(k)}$, respectively. The equation to find the increments is

$$\left\{ \begin{bmatrix} \mathbf{k}_{I,e} & -\mathbf{k}_{I,e} \\ -\mathbf{k}_{I,e} & \mathbf{k}_{I,e} \end{bmatrix} + \begin{bmatrix} \mathbf{0} & \mathbf{0} \\ \mathbf{0} & {}^t \mathbf{k}_{T,e}^{\text{struct},(k-1)} \end{bmatrix} \right\} \begin{bmatrix} \Delta \mathbf{u}_{e,\text{out}}^{(k)} \\ \Delta \mathbf{u}_{e,\text{in}}^{(k)} \end{bmatrix} = \begin{bmatrix} \mathfrak{R}_{e,\text{out}}^{(k-1)} \\ \mathfrak{R}_{e,\text{in}}^{(k-1)} \end{bmatrix}, \quad (7)$$

with

$$\mathbf{k}_{I,e} = l_e(\gamma_e) \mathbf{I}_{8 \times 8}, \quad (8)$$

where $\mathbf{0}$ and $\mathbf{I}_{8 \times 8}$ are the 8×8 zero matrix and identity matrix (in the two-dimensional case).

The link stiffness of the e -th patch, l_e , is a function of the design variable. The stiffness matrix, the residual force terms of the outer and the inner nodes of the e -th patch are denoted by ${}^t \mathbf{k}_{T,e}^{\text{struct},(k-1)}$, $\mathfrak{R}_{e,\text{out}}^{(k-1)}$ and $\mathfrak{R}_{e,\text{in}}^{(k-1)}$, respectively. The force terms $\mathfrak{R}_{e,\text{out}}^{(k-1)}$ and $\mathfrak{R}_{e,\text{in}}^{(k-1)}$ are calculated as

$$\begin{bmatrix} \mathfrak{R}_{e,\text{out}}^{(k-1)} \\ \mathfrak{R}_{e,\text{in}}^{(k-1)} \end{bmatrix} = \begin{bmatrix} {}^{t+\Delta t} \mathbf{R}_e \\ \mathbf{0} \end{bmatrix} - \begin{bmatrix} \mathbf{0} \\ {}^{t+\Delta t} \mathbf{f}_e^{\text{struct},(k-1)} \end{bmatrix} - \begin{bmatrix} {}^{t+\Delta t} \mathbf{f}_{e,\text{out}}^{\text{link},(k-1)} \\ {}^{t+\Delta t} \mathbf{f}_{e,\text{in}}^{\text{link},(k-1)} \end{bmatrix}, \quad (9)$$

$$\begin{bmatrix} {}^{t+\Delta t} \mathbf{f}_{e,\text{out}}^{\text{link},(k-1)} \\ {}^{t+\Delta t} \mathbf{f}_{e,\text{in}}^{\text{link},(k-1)} \end{bmatrix} = \begin{bmatrix} \mathbf{k}_{I,e} & -\mathbf{k}_{I,e} \\ -\mathbf{k}_{I,e} & \mathbf{k}_{I,e} \end{bmatrix} \begin{bmatrix} {}^{t+\Delta t} \mathbf{u}_{e,\text{out}}^{(k-1)} \\ {}^{t+\Delta t} \mathbf{u}_{e,\text{in}}^{(k-1)} \end{bmatrix}. \quad (10)$$

In (9), the externally applied force on the outer nodes is denoted by ${}^{t+\Delta t} \mathbf{R}_e$ and the internal force acting on the inner nodes by ${}^{t+\Delta t} \mathbf{f}_e^{\text{struct},(k-1)}$. By applying the static condensation strategy, the degrees related to the inner nodes are condensed out, leading to

$${}^t \mathbf{k}_{\text{Con},e}^{(k-1)} \Delta \mathbf{u}_{e,\text{out}}^{(k)} = \mathfrak{R}_{e,\text{out}}^{(k-1)} + \mathbf{k}_{I,e} (\mathbf{k}_{I,e} + {}^t \mathbf{k}_{T,e}^{\text{struct},(k-1)})^{-1} \mathfrak{R}_{e,\text{in}}^{(k-1)}, \quad (11)$$

where

$${}^t \mathbf{k}_{\text{Con},e}^{(k-1)} = (\mathbf{k}_{I,e} - \mathbf{k}_{I,e} (\mathbf{k}_{I,e} + {}^t \mathbf{k}_{T,e}^{\text{struct},(k-1)})^{-1} \mathbf{k}_{I,e}). \quad (12)$$

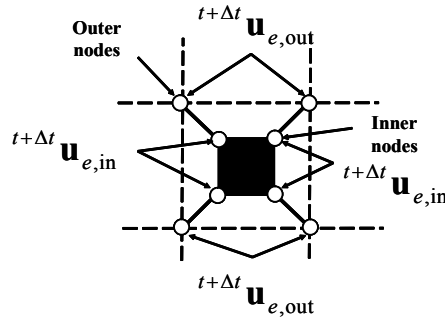


Figure 3. The e -th patch surrounding the e -th element for the ECP method. The inner nodes are the nodes defining the element while the outer nodes defining the e -th patch are used to connect patches sharing the same outer nodes. The solid lines connecting the inner and outer nodes denote zero-length one-dimensional elastic links.

Then the global tangent matrix is assembled as

$${}^t\mathbf{K}_{\text{Con}}^{(k-1)} = \sum_{e=1}^{N_p} {}^t\mathbf{k}_{\text{Con},e}^{(k-1)}, \quad (13)$$

where N_p is the total number of patches. Finally, the following system of equations is solved iteratively by a standard nonlinear solver such as the Newton–Raphson method or the arc-length method:

$${}^t\mathbf{K}_{\text{Con}}^{(k-1)} \Delta \mathbf{U}_{\text{out}}^{(k)} = \mathfrak{R}_{\text{Con}}^{(k-1)} \quad (14)$$

where

$$\mathfrak{R}_{\text{Con}}^{(k-1)} = \sum_{e=1}^{N_p} (\mathfrak{R}_{e,\text{out}}^{(k-1)} + \mathbf{k}_{I,e}(\mathbf{k}_{I,e} + {}^t\mathbf{k}_{T,e}^{\text{struct},(k-1)})^{-1} \mathfrak{R}_{e,\text{in}}^{(k-1)}) \quad (15)$$

For efficient topology optimization procedures, it is crucial to use an appropriate interpolation function for the ECP method. In this paper, the following interpolation function is adopted for the link stiffness in (8):

$$\text{Solid: } l_e = l_{\max}, \quad \gamma_e = 1, \quad (16)$$

$$\text{Void: } l_e = l_{\min}, \quad \gamma_e = 0.001, \quad (17)$$

$$l_e = \alpha \frac{\gamma_e^n}{1 + (1 - \gamma_e^n)\tau} + \beta \left(\tau = \frac{\alpha \times s}{k_{\text{diagonal}}^{\text{struct}} \times k} \right), \quad (18)$$

$$\alpha = l_{\max} - l_{\min}, \quad \beta = l_{\min}, \quad (19)$$

$$\gamma_{\min} \leq \gamma_e \leq 1, \quad \gamma_{\min} = 0.001, \quad (20)$$

where k is the number of degrees of freedom per node and s and n are penalty parameters. A diagonal term of the linear stiffness matrix is denoted by $k_{\text{diagonal}}^{\text{struct}}$. The upper and lower bounds of the stiffness of links are denoted by l_{\max} and l_{\min} , respectively. Here, l_{\max} and l_{\min} are set to $10^6 \times k_{\text{diagonal}}^{\text{struct}}$ and $10^{-6} \times k_{\text{diagonal}}^{\text{struct}}$, respectively. (See [Yoon et al. 2007; Yoon et al. 2008; Yoon 2010] for more details on the interpolation function adopted above and actual implementation on Matlab.)

3. Topology optimization formulation

3.1. Optimization formulation. To find a structural layout tracing a given load-displacement trajectory, the following optimization formulation is considered, where nl is the number of loadsteps and N_p is the number of discretizing patches:

$$\text{Min}_{\gamma} \Phi = \sum_{i=1}^{nl} \left\| \mathbf{L}_d^T {}^{t+\Delta t} \mathbf{U}^i - {}^{t+\Delta t} \mathbf{U}^{i,\text{ref}} \right\| \quad (21)$$

$$\text{s. t. } \sum_{e=1}^{N_p} \rho_e(\gamma_e) v_e \leq V^*, \quad (22)$$

with $\gamma = \{\gamma_1, \gamma_2, \dots, \gamma_{N_p}\}^T$. Here Φ is a scalar objective function measuring the sum of the differences between the actual displacements ${}^{t+\Delta t}\mathbf{U}^i$ and the target displacement ${}^{t+\Delta t}\mathbf{U}^{i,\text{ref}}$ for nl steps for a given load. The symbol \mathbf{L}_d denotes a vector which has unity at the node of the displacement measurement point and all zeros for the rest. The density and element volume of the e -th patch are denoted by ρ_e and v_e , respectively. The prescribed volume limit is V^* . Instead of the objective function in (21), one may prescribe a displacement path and calculate the reaction force as the response. In this case, the objective function Φ is defined as

$$\Phi = \sum_{i=1}^{nl} \left\| \mathbf{L}_r^T {}^{t+\Delta t}\mathbf{F}_{\text{Int}}^i - {}^{t+\Delta t}\mathbf{R}^{i,\text{ref}} \right\|, \quad (23)$$

where ${}^{t+\Delta t}\mathbf{R}^{i,\text{ref}}$ and ${}^{t+\Delta t}\mathbf{F}_{\text{Int}}^i$ are the target reaction force and the internal force vector at the i -th load step of the Newton–Raphson iteration. The symbol \mathbf{L}_r is a vector which has unity at the node of the reaction force measurement point and all zeros for the rest.

The objective function in (23) was used by [Sekimoto and Noguchi 2001] to find optimal layouts satisfying a prescribed load-displacement trajectory. Theoretically, the use of either (21) or (23) would yield the same result (layout) if the same load-displacement trajectory is pursued. However, when the load-displacement trajectory becomes complex, the displacement control procedure is known to perform better in convergence. Although it can fail for a complex trajectory such as those involving snap-backs and/or snap-through phenomena, the displacement control procedure usually works better than the load control procedure using the objective function of (23) [Bathe 1996; Hellweg and Crisfield 1998; Liu and Nocedal 1989; Vila et al. 1997; Cook et al. 2001]. So it is implemented in the Newton–Raphson nonlinear solver for this investigation.

Although the functional form of (23) is used, there might be alternatives in selecting the specific norm. For instance, one can consider the Euclidean norm (2-norm)

$$\Phi = \sum_{i=1}^{nl} (\mathbf{L}_r^T {}^{t+\Delta t}\mathbf{F}_{\text{Int}}^i - {}^{t+\Delta t}\mathbf{R}^{i,\text{ref}})^2, \quad (24)$$

the p -norm

$$\Phi = \left(\sum_{i=1}^{nl} (\mathbf{L}_r^T {}^{t+\Delta t}\mathbf{F}_{\text{Int}}^i - {}^{t+\Delta t}\mathbf{R}^{i,\text{ref}})^p \right)^{1/p} \quad (p = 2, 4, 6, \dots), \quad (25)$$

or the maximum norm

$$\Phi = \max(|\mathbf{L}_r^T {}^{t+\Delta t}\mathbf{F}_{\text{Int}}^i - {}^{t+\Delta t}\mathbf{R}^{i,\text{ref}}|). \quad (26)$$

Obviously, the optimization convergence can be affected by the choice of the norm. The use of the Euclidean norm is to minimize the sum of every distance between the response reaction force and the reference (target) force for all incremental steps. On the other hand, the maximum norm minimizes the maximum distance. For example, let us consider an intermediate design for which the reaction follows the trajectory depicted in Figure 4. With the Euclidean norm, the average square of distances (the area marked by A) is to be minimized. With the p -norm with a sufficient large p or the maximum norm, the distance at load step 3 is minimized because the distance of the load step 3 (the vertical distance marked

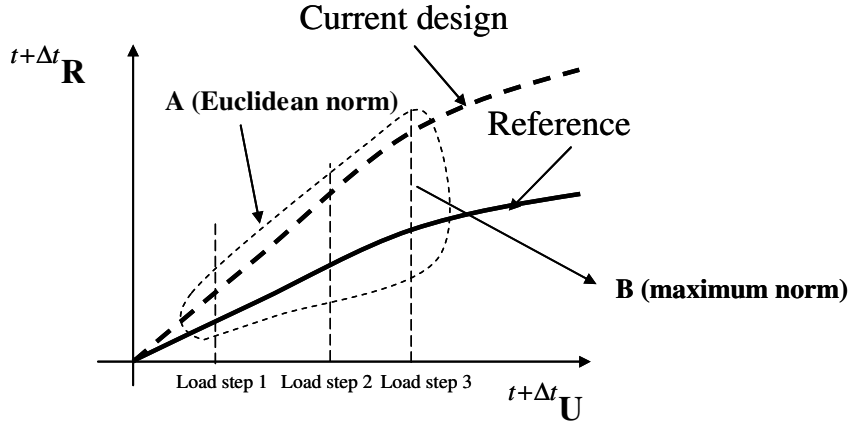


Figure 4. A typical load-displacement trajectory at an intermediate design step.

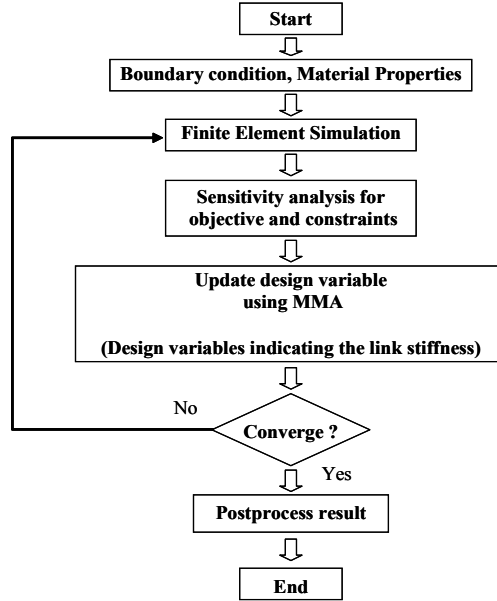


Figure 5. Topology design optimization procedure.

by B) is the largest. It is often useful to normalize the aforementioned norms as

$$\Phi = \sum_{i=1}^{nl} \left(\frac{\mathbf{L}_r^T \mathbf{t} + \Delta t \mathbf{F}_{\text{Int}}^i}{\mathbf{t} + \Delta t \mathbf{R}^{i,\text{ref}}} - 1 \right)^2, \quad \Phi = \left(\sum_{i=1}^{nl} \left(\frac{\mathbf{L}_r^T \mathbf{t} + \Delta t \mathbf{F}_{\text{Int}}^i}{\mathbf{t} + \Delta t \mathbf{R}^{i,\text{ref}}} - 1 \right)^p \right)^{1/p}, \quad \Phi = \max \left(\left| \frac{\mathbf{L}_r^T \mathbf{t} + \Delta t \mathbf{F}_{\text{Int}}^i}{\mathbf{t} + \Delta t \mathbf{R}^{i,\text{ref}}} - 1 \right| \right). \quad (27)$$

In general, it is difficult to judge in advance which norm would perform better for a given problem. Therefore, one may test various norms as given by (24)–(27) before finding optimal solutions. Figure 5 depicts an implemented topology optimization procedure to find a structure tracing a specific load-displacement trajectory.

3.2. Sensitivity analysis. To update the design variables ($\gamma = \{\gamma_1, \gamma_2, \dots, \gamma_{Np-1}, \gamma_{Np}\}^T$), the optimization procedure as described in Figure 5 will be employed. To obtain the sensitivity of the objective function Φ with respect to the design variable, γ , it is necessary to derive the sensitivities of the displacement or the reaction force depending on the form of the selected objective function. Although the procedure to calculate the sensitivity for the present ECP method may be similar to that based on the element density method, it is worth giving it in some detail. For analysis, we assume that the size of the degrees of freedom of displacement is n_G and the displacement conditions (condensed degrees of freedom) are applied at ${}^{t+\Delta t}\mathbf{U}_{kn}$ where ${}^{t+\Delta t}\mathbf{U}_{un}$ denotes the unknown displacements (to be determined by a nonlinear solver). So the following definitions are introduced for the sensitivity analysis:

$$\Psi_d = \mathbf{L}_d^T {}^{t+\Delta t}\mathbf{U}, \quad \Psi_r = \mathbf{L}_r^T {}^{t+\Delta t}\mathbf{F}_{int, kn},$$

where \mathbf{L}_d and \mathbf{L}_r are $n_G \times 1$ and $n_{kn} \times 1$ vectors for the temporarily objective functions Ψ_d and Ψ_r of the displacement and the reaction force, respectively. By separating the known displacements from unknown displacements, one can express the governing equation by using the residual vector:

$$\mathfrak{R} = {}^{t+\Delta t}\mathbf{F}_{Ext} - {}^{t+\Delta t}\mathbf{F}_{Int} = \begin{bmatrix} {}^{t+\Delta t}\mathbf{F}_{Ext, un} - {}^{t+\Delta t}\mathbf{F}_{Int, un} \\ {}^{t+\Delta t}\mathbf{F}_{Ext, kn} - {}^{t+\Delta t}\mathbf{F}_{Int, kn} \end{bmatrix} = \begin{bmatrix} \mathbf{0}_{un \times 1} \\ \mathbf{0}_{kn \times 1} \end{bmatrix} \quad (28)$$

Because the boundary conditions are specified on ${}^{t+\Delta t}\mathbf{U}_{kn}$, the second row of the above equation can be removed. Without the loss of generality, the load step index appearing as a right superscript is omitted.

3.3. Sensitivity of the displacement. The sensitivity of Ψ_d with respect to the design variable γ requires the sensitivity of the displacement ${}^{t+\Delta t}\mathbf{U}$:

$$\Psi'_d = \mathbf{L}_d^T {}^{t+\Delta t}\mathbf{U}' \quad (29)$$

where differentiation is with respect to γ . To calculate ${}^{t+\Delta t}\mathbf{U}'$, the equilibrium equation, $\mathfrak{R} = \mathbf{0}_{n_G \times 1}$, is differentiated:

$$\frac{\partial \mathfrak{R}}{\partial {}^{t+\Delta t}\mathbf{U}} \frac{\partial {}^{t+\Delta t}\mathbf{U}}{\partial \gamma} + \mathfrak{R}' = \mathbf{0}_{n_G \times Np}. \quad (30)$$

If an adjoint variable $\boldsymbol{\lambda}$ is solved from

$$\frac{\partial \mathfrak{R}}{\partial {}^{t+\Delta t}\mathbf{U}} \boldsymbol{\lambda} = \mathbf{L}_d, \quad (31)$$

the sensitivity Ψ'_d can be easily found from

$$\Psi'_d = -\boldsymbol{\lambda}^T \mathfrak{R}'. \quad (32)$$

3.4. Sensitivity of the reaction force. The sensitivity of Ψ_r with respect to the design variable γ can be obtained by a technique similar to that used to calculate Ψ'_d . For the displacement-controlled case, it is convenient to put ${}^{t+\Delta t}\mathbf{U}$ as

$${}^{t+\Delta t}\mathbf{U} = [{}^{t+\Delta t}\mathbf{U}_{un}, {}^{t+\Delta t}\mathbf{U}_{kn}]^T \quad (33)$$

In this case, the residual vector \mathfrak{R} can be also put as

$$\mathfrak{R} = \begin{bmatrix} {}^{t+\Delta t}\mathbf{F}_{\text{Ext},un} \\ \mathbf{0}_{kn \times 1} \end{bmatrix} - \begin{bmatrix} {}^{t+\Delta t}\mathbf{F}_{\text{Int},un} \\ {}^{t+\Delta t}\mathbf{F}_{\text{Int},kn} \end{bmatrix} = \begin{bmatrix} \mathbf{0}_{un \times 1} \\ \mathbf{0}_{kn \times 1} \end{bmatrix}, \quad \frac{\partial^{t+\Delta t}\mathbf{F}_{\text{Int}}}{\partial^{t+\Delta t}\mathbf{U}} = \begin{bmatrix} \frac{\partial^{t+\Delta t}\mathbf{F}_{\text{Int},un}}{\partial^{t+\Delta t}\mathbf{U}_{un}} & \frac{\partial^{t+\Delta t}\mathbf{F}_{\text{Int},un}}{\partial^{t+\Delta t}\mathbf{U}_{kn}} \\ \frac{\partial^{t+\Delta t}\mathbf{F}_{\text{Int},kn}}{\partial^{t+\Delta t}\mathbf{U}_{un}} & \frac{\partial^{t+\Delta t}\mathbf{F}_{\text{Int},kn}}{\partial^{t+\Delta t}\mathbf{U}_{kn}} \end{bmatrix}. \quad (34)$$

First, we differentiate Ψ_r :

$$\frac{d\Psi_r}{d\gamma} = \mathbf{L}_r^T \left(\frac{\partial^{t+\Delta t}\mathbf{F}_{\text{Int},kn}}{\partial^{t+\Delta t}\mathbf{U}_{un}} \frac{\partial^{t+\Delta t}\mathbf{U}_{un}}{\partial\gamma} + \frac{\partial^{t+\Delta t}\mathbf{F}_{\text{Int},kn}}{\partial^{t+\Delta t}\mathbf{U}_{kn}} \frac{\partial^{t+\Delta t}\mathbf{U}_{kn}}{\partial\gamma} + \frac{\partial^{t+\Delta t}\mathbf{F}_{\text{Int},kn}}{\partial\gamma} \right). \quad (35)$$

Because ${}^{t+\Delta t}\mathbf{U}_{un} = {}^{t+\Delta t}\mathbf{U}^*$ (condensed degrees of freedom), the second term in parenthesis in (35) vanishes: $\partial^{t+\Delta t}\mathbf{U}_{kn}/\partial\gamma = \mathbf{0}_{kn \times Np}$. To calculate the first term, the equilibrium equation (34) is differentiated:

$$\frac{\partial^{t+\Delta t}\mathbf{F}_{\text{Ext},un}}{\partial\gamma} - \frac{\partial^{t+\Delta t}\mathbf{F}_{\text{Int},un}}{\partial^{t+\Delta t}\mathbf{U}_{un}} \frac{\partial^{t+\Delta t}\mathbf{U}_{un}}{\partial\gamma} - \frac{\partial^{t+\Delta t}\mathbf{F}_{\text{Int},un}}{\partial\gamma} = \mathbf{0}_{un \times Np}. \quad (36)$$

By inserting (36) into (35), we obtain

$$\begin{aligned} \frac{\partial\Psi_r}{\partial\gamma} &= \mathbf{L}_r^T \left(\frac{\partial^{t+\Delta t}\mathbf{F}_{\text{Int},kn}}{\partial^{t+\Delta t}\mathbf{U}_{un}} \left(\left(\frac{\partial^{t+\Delta t}\mathbf{F}_{\text{Int},un}}{\partial^{t+\Delta t}\mathbf{U}_{un}} \right)^{-1} \left(\frac{\partial^{t+\Delta t}\mathbf{F}_{\text{Ext},un}}{\partial\gamma} - \frac{\partial^{t+\Delta t}\mathbf{F}_{\text{Int},un}}{\partial\gamma} \right) + \frac{\partial^{t+\Delta t}\mathbf{F}_{\text{Int},kn}}{\partial\gamma} \right) \right) \\ &= \mathbf{L}_r^T \left[-\frac{\partial^{t+\Delta t}\mathbf{F}_{\text{Int},kn}}{\partial^{t+\Delta t}\mathbf{U}_{un}} \left(\frac{\partial^{t+\Delta t}\mathbf{F}_{\text{Int},un}}{\partial^{t+\Delta t}\mathbf{U}_{un}} \right)^{-1} \mathbf{I}_{kn \times Np} \right] \begin{bmatrix} -\frac{\partial^{t+\Delta t}\mathbf{F}_{\text{Ext},un}}{\partial\gamma} + \frac{\partial^{t+\Delta t}\mathbf{F}_{\text{Int},un}}{\partial\gamma} \\ \frac{\partial^{t+\Delta t}\mathbf{F}_{\text{Int},kn}}{\partial\gamma} \end{bmatrix}. \end{aligned} \quad (37)$$

We now introduce the adjoint variable $\boldsymbol{\lambda}$, with $\boldsymbol{\lambda}^T \equiv [\boldsymbol{\lambda}_{un} \ \boldsymbol{\lambda}_{kn}]^T$, where $\boldsymbol{\lambda}_{kn} = \mathbf{L}_r$, and simplify (37) to

$$\frac{\partial\Psi_r}{\partial\gamma} = \boldsymbol{\lambda}^T \begin{bmatrix} -\frac{\partial^{t+\Delta t}\mathbf{F}_{\text{Ext},un}}{\partial\gamma} + \frac{\partial^{t+\Delta t}\mathbf{F}_{\text{Int},un}}{\partial\gamma} \\ \frac{\partial^{t+\Delta t}\mathbf{F}_{\text{Int},kn}}{\partial\gamma} \end{bmatrix}, \quad (38)$$

$$\begin{bmatrix} \frac{\partial^{t+\Delta t}\mathbf{F}_{\text{Int},un}}{\partial^{t+\Delta t}\mathbf{U}_{un}} & \frac{\partial^{t+\Delta t}\mathbf{F}_{\text{Int},un}}{\partial^{t+\Delta t}\mathbf{U}_{kn}} \\ \frac{\partial^{t+\Delta t}\mathbf{F}_{\text{Int},kn}}{\partial^{t+\Delta t}\mathbf{U}_{un}} & \frac{\partial^{t+\Delta t}\mathbf{F}_{\text{Int},kn}}{\partial^{t+\Delta t}\mathbf{U}_{kn}} \end{bmatrix} \begin{bmatrix} \boldsymbol{\lambda}_{un} \\ \boldsymbol{\lambda}_{kn} \end{bmatrix} = \begin{bmatrix} \mathbf{0}_{un \times 1} \\ \mathbf{0}_{kn \times 1} \end{bmatrix}. \quad (39)$$

Since $\boldsymbol{\lambda}_{kn} = \mathbf{L}_r$, this leads to

$$\boldsymbol{\lambda} = \begin{bmatrix} -\left(\frac{\partial^{t+\Delta t}\mathbf{F}_{\text{Int},un}}{\partial^{t+\Delta t}\mathbf{U}_{un}} \right)^{-1} \frac{\partial^{t+\Delta t}\mathbf{F}_{\text{Int},kn}}{\partial^{t+\Delta t}\mathbf{U}_{kn}} \mathbf{L}_r \\ \mathbf{L}_r \end{bmatrix}. \quad (40)$$

The validity of the sensitivity analysis was checked against the direct numerical result by finite difference.

4. Examples of topology optimization

This paper considers problems defined only in two-dimensional domains, but the validity and efficiency of the ECP-based solution approach can be clearly demonstrated in the topology optimization tracing given load-displacement curves. It is noted that the developed ECP-based approach does not entail any special treatment or tuning for stabilizing possible instability in the Newton–Raphson iterations or in optimization processes. Because the ECP method is used here, all the remarks and findings are mainly applicable to an approach based on the ECP method, not on the element density method. One may see more detailed explanations of the advantages and drawbacks of the element density method for some nonlinear problems may be found in [Buhl et al. 2000; Bruns and Tortorelli 2003; Cho and Jung 2003; Yoon and Kim 2005b; Yoon et al. 2008]. Unless stated otherwise, uniform initial guesses of γ satisfying given mass constraints are used. The dimension, material properties and magnitude of the loads are so chosen as to demonstrate the potential of the present ECP based formulation. In this study, the method of moving asymptotes is used as an optimization algorithm [Svanberg 1987]; however other optimization algorithms can also be used.

Example 1: Controlling the load-displacement curve. As the first numerical example, we consider the problem depicted in Figure 6a. The design domain is discretized by 60×40 four-node quad elements. The displacement is prescribed at the top-right node while other boundary conditions are depicted in the figure. Young’s modulus and Poisson’s ratio are set to be 1 N/m^2 and 0.4, respectively.

Before solving the optimization problem set up as (21) and (22), a nominal structure maximizing the reaction force for a specified displacement value where the structural response is found by using linear strains. The result is shown in Figure 6b, which should be the same as the result obtained by a standard compliance minimization using linear strains. To obtain the result in Figure 6b, the sensitivity filter of radius equal to 1.2 times the element size was used [Bendsøe and Sigmund 2003].

It will be interesting to investigate the load-displacement trajectory when the geometric nonlinearity using the Green–Lagrangian strain is used for the optimized layout of Figure 6b. The result is given in Figure 6c for which the maximum tip displacement δ_{\max} is set to be 0.12 m. When the nonlinearity is considered, the drop in the reaction force is expected as the tip displacement (δ) reaches δ_{\max} . This is due to a buckling phenomenon caused by the local bending indicated in Figure 6d.

Now let us try to find a structural layout following a prescribed load-displacement trajectory based on geometric nonlinear analysis. By using the trajectory in Figure 6c as a nominal trajectory, we set up a problem to find a structure that passes the following two points in the load-displacement trajectory:

$$\text{Target: } \begin{cases} {}^{t+\Delta t} \mathbf{R}^{1,\text{ref}} = 1.0 \times 10^{-3} \text{ N at } \delta = 0.06 \text{ m,} \\ {}^{t+\Delta t} \mathbf{R}^{2,\text{ref}} = 2.0 \times 10^{-3} \text{ N at } \delta = 0.12 \text{ m.} \end{cases} \quad (41)$$

The load-displacement relation required by (41) states that the target structure should not exhibit apparent weakening effects near 0.12 m for the input displacement because ${}^{t+\Delta t} \mathbf{R}^{2,\text{ref}}$ by (41) is larger than the corresponding value predicted in Figure 6c. In other words, the overall stiffness before 0.6 m of the input displacement should be smaller than that of the linear design but a sudden drop due to the geometric weakening in the reaction force observed at the linear design can be avoided at $\delta = 0.12 \text{ m}$ if a structure satisfying (41) is indeed found.

By using the optimization formulation of (22) and (23) (with $V^* = 20\%$ as before), the optimized layouts tracing the target response of (41) are shown in Figure 7, left and middle. In defining (23), the Euclidean norm defined in (24) was used. The fixed filter implies the sensitivity filter using the fixed radius (r_{filter}) of 1.2 times the element size while the varying filter implies the sensitivity filter using the following filter radius (this can be viewed as a special case of the continuation method):

$$r_{\text{filter}} = \begin{cases} 1.2 \times \text{element size} & \text{for loop} \leq 150 \text{ iterations,} \\ 1.0 \times \text{element size} & \text{for loop} > 150 \text{ iterations.} \end{cases} \quad (42)$$

The main motivation to use the varying filter is to minimize the appearance of intermediate density elements because the existence of these elements can significantly affect structural response especially when nonlinear analysis is considered.

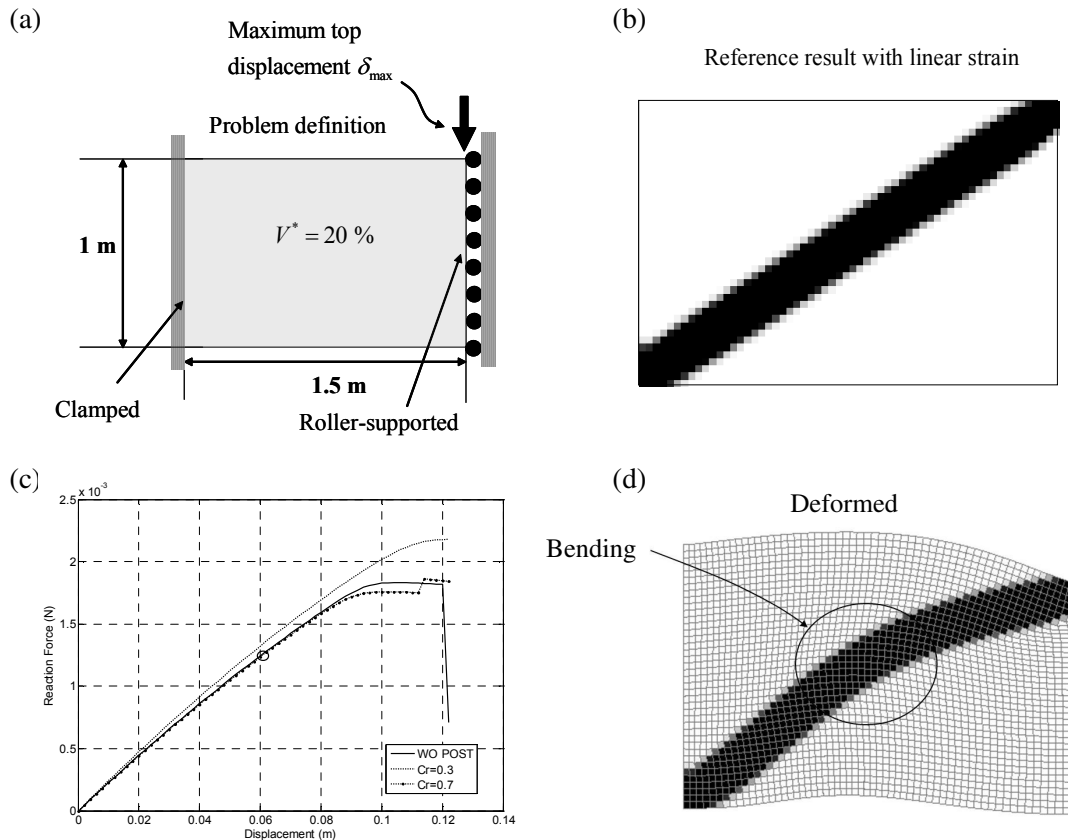


Figure 6. A test problem. (a) Problem definition ($E=1 \text{ N/m}^2$, $\nu = 0.4$). (b) Optimized layout for $V^* = 20\%$ when linear analysis is used. (c) Load-displacement trajectory of the layout in (b) by geometrically nonlinear analysis; Cr is the threshold design variable value for hard-kill postprocessing. (d) Deformed shape by nonlinear analysis when the top displacement reaches 0.12 m.

To check the effects of postprocessing, for instance, Figure 6c compares the load-displacement curves before and after the hard-kill postprocessing by which the elements having design variables above or equal a threshold Cr are replaced by solid elements, and elements having the design variables lower than Cr by void elements. Two values of Cr were used: 0.3 and 0.7. As seen from Figure 6c, the differences among the responses can be neglected in the linear range but become significant in the nonlinear range. As a result, more effort should be made to avoid intermediate design values but the optimized layouts in existing works dealing with nonlinear load-displacement curve tracing seem to contain quite a large portion of intermediate variables. As shall be seen later with numerical results, the optimized layouts by the element connectivity method appear to have a smaller portion of intermediate variables.

Although the filter-size varying technique helped to reduce the occurrence of intermediate density elements, they were not completely removed. The load-displacement trajectories by the optimized layouts are plotted in Figure 7, right. Note that an additional member has appeared in the optimized layouts when the target trajectory is required to pass two reference points in (41). When δ exceeds $\delta_{max} = 0.12\text{m}$, the reaction forces suddenly drop and the response pattern is significantly affected even by small differences in the layout configuration, which may be viewed as an imperfection.

Now let us find a structural layout to follow the load-displacement trajectories having slightly different reference points from those used to obtain the layouts in Figure 7. Among others, the value of the reaction force at $\delta = 0.06\text{m}$ is varied. The comparison of the obtained layouts in Figure 8a,b and that shown in Figure 8c indicates that the member starting at A should be more straight as a larger reaction force at $\delta = 0.06\text{m}$ is required. As a larger reaction force is required at $\delta = 0.06\text{m}$, the reduction in the tangent stiffness of the obtained layout at $\delta = 0.12\text{m}$ is more significant. Another observation is that it may be not always possible to obtain a layout yielding a given load-displacement trajectory passing through arbitrarily specified load-displacement points because there may not exist such a layout. For instance, the trajectory marked by (a) in the graph of Figure 8 does not exactly pass through $({}^{t+\Delta t}\mathbf{R}^{2,\text{ref}}, \delta) = (2.0 \times 10^{-3}\text{N}, 0.12\text{m})$.

Furthermore, to prevent the sudden drop of the reaction force of the design in Figure 8c near $\delta = 0.144\text{m}$, the one reference point at $\delta = 0.144\text{m}$ in Figure 9 is additionally inserted and the effect of this inclusion is tested. The changes of the details of the design of Figure 8c are observed in Figure 9.

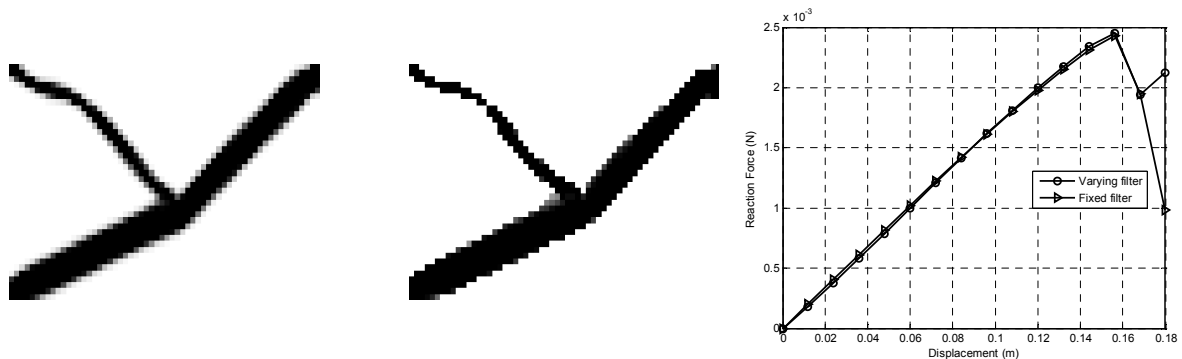


Figure 7. Layout optimization following the specific target reference points in the load-displacement trajectory: optimized layouts using fixed filter (left) and varying filter (middle); load-displacement trajectories for the optimized layouts (right).

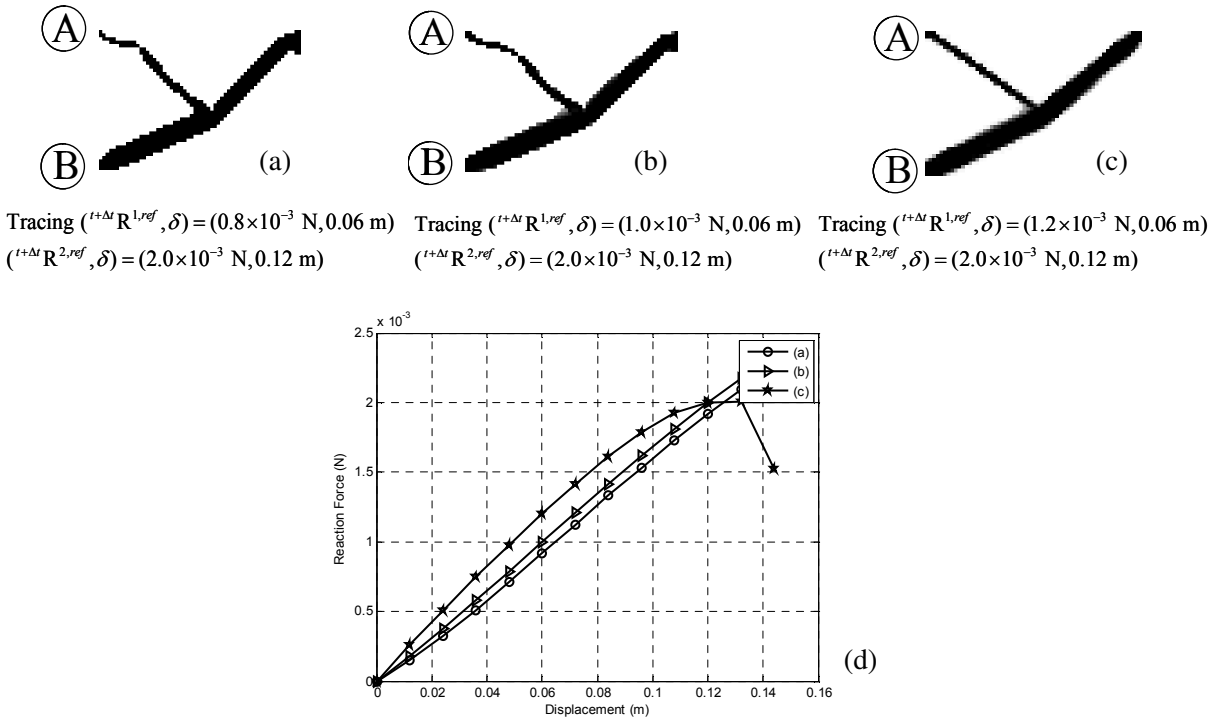


Figure 8. Top: optimized layouts following different target reference points in the load-displacement trajectory. Bottom: corresponding load-displacement trajectories.

The straight line near the point A becomes thicker and the straight line near the point C becomes narrow compared with the design in Figure 8c. This reveals that the ECP based topology optimization can change the details of the design to satisfy the given load and displacement curve. Furthermore, it proves that after the post processing of obtained layouts, the size or shape optimization process may be required to compensate the adverse effect of the postprocessing.

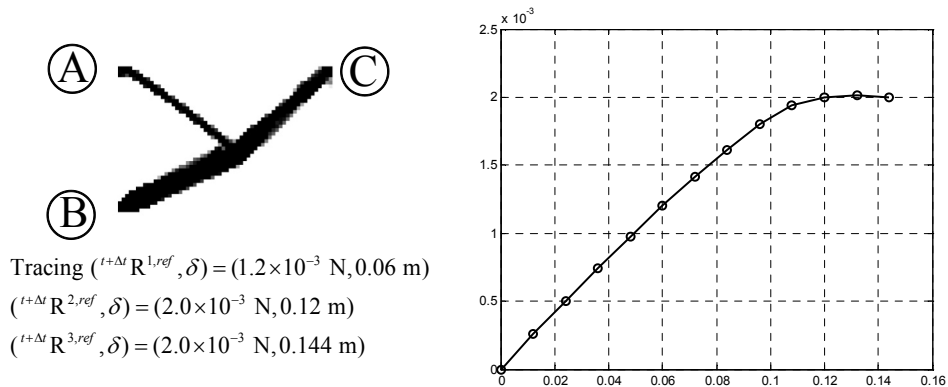


Figure 9. Optimization test by including an additional point for the design of Figure 8c: design (left) and load-displacement curve (right).

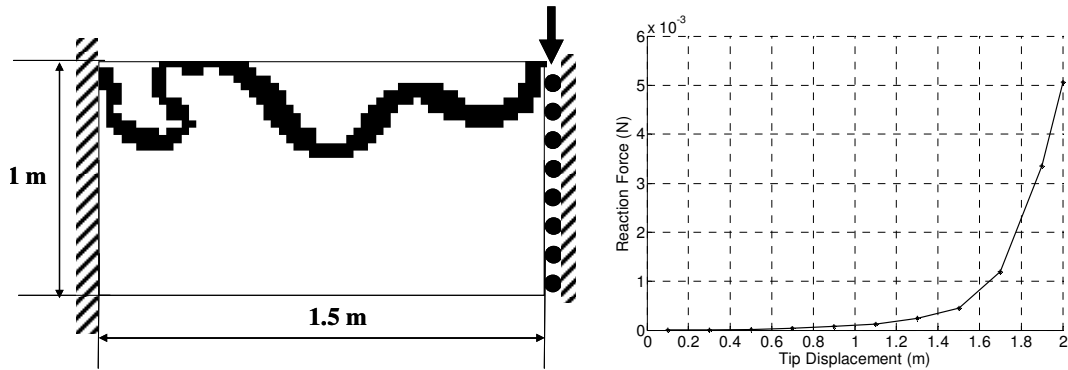


Figure 10. Left: reference layout. Right: load-displacement trajectory.

The normalized norm was also considered in the definition of the objective function. Although the optimized results are not shown, the layout configurations with and without the normalization were not much different. For this reason, the unnormalized Euclidean norm defined in (24) will be used in the subsequent examples.

Example 2: Design of a stiffening structure. To test if the proposed formulation can find a structural layout exhibiting geometrical stiffening behavior, a structure shown in Figure 10 is devised. When the structure is loaded at the tip marked by a vertical arrow, it exhibits geometrical stiffening. Note that the stiffening effect results from the constraint of the horizontal displacement along the roller support. The optimization problem considered is to recover the layout shown in Figure 10, left, when the curve in Figure 10, right, is given as the target trajectory. To solve this problem, the formulation given by (22) and (23) is adopted. Eleven points in the load-displacement curves marked by dots in Figure 10, right, are used. The intermediate and final layouts appearing during optimization iterations and the corresponding load-displacement trajectories are shown in Figure 11, which indicates that the proposed

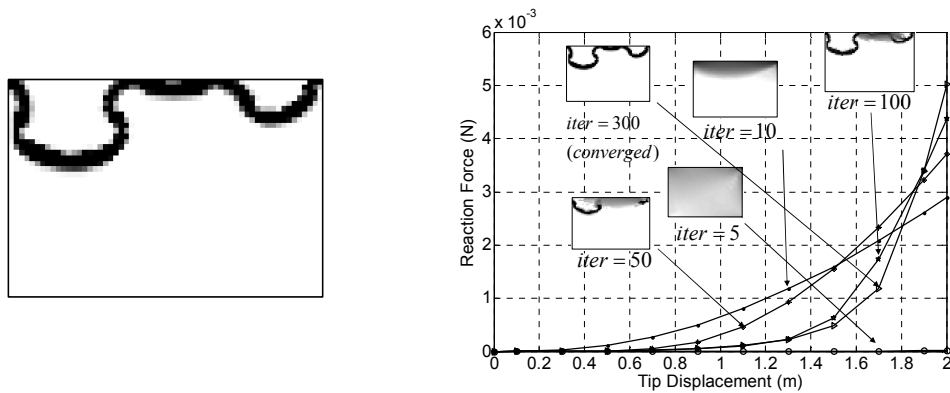


Figure 11. Optimized results by the developed method in recovering the reference layout exhibiting the nonlinear load-displacement curve in Figure 10. Left: the optimized layout. Right: load-displacement curves of the intermediate and final layouts.

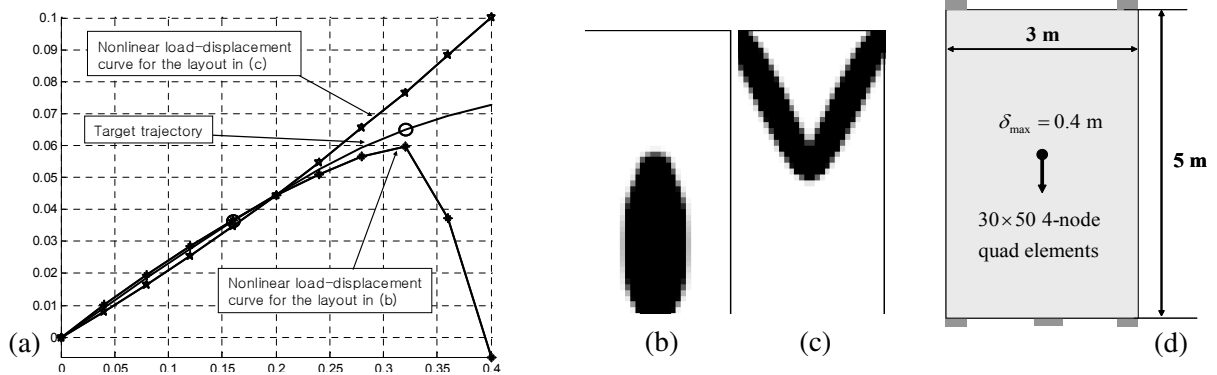


Figure 12. A problem to find a target nonlinear load-displacement trajectory. Left: target and limiting trajectories. Middle: reference layouts yielding linear and nonlinear limiting trajectories. Right: a compliance minimization problem used to obtain the given layouts with $E = 1 \text{ N/m}^2$, $\nu = 0.4$, volume = 20%.

ECP-based formulation is capable of finding a layout very close to the one given in Figure 10, left, while the specified load-displacement curve is fairly accurately traced.

Example 3: Center-loaded structure with a specified structural response. Here, we look for a structural layout following a target load-displacement trajectory in Figure 12a, lying between two limiting trajectories. The limiting trajectories shown in the graph are the trajectories of the layouts (b) and (c) in Figure 12, optimized through compliance minimization (defined in Figure 12d) by using linear and geometrically nonlinear analyses. In obtaining the layouts, the center of the design domain was pulled down by $\delta_{max} = 0.4$ m and a checkerboard filter of radius equal to 1.2 times the element size was used.

To solve this problem, $nl = 2$ was used and the specific reference points were $({}^{t+\Delta t}\mathbf{R}^{1,ref}, \delta) = (0.0363 \text{ N}, 0.16 \text{ m})$ and $({}^{t+\Delta t}\mathbf{R}^{2,ref}, \delta) = (0.065 \text{ N}, 0.32 \text{ m})$. Figure 13 shows the optimized result for this problem. The optimized layout (left) and the variation of the load-displacement trajectories are

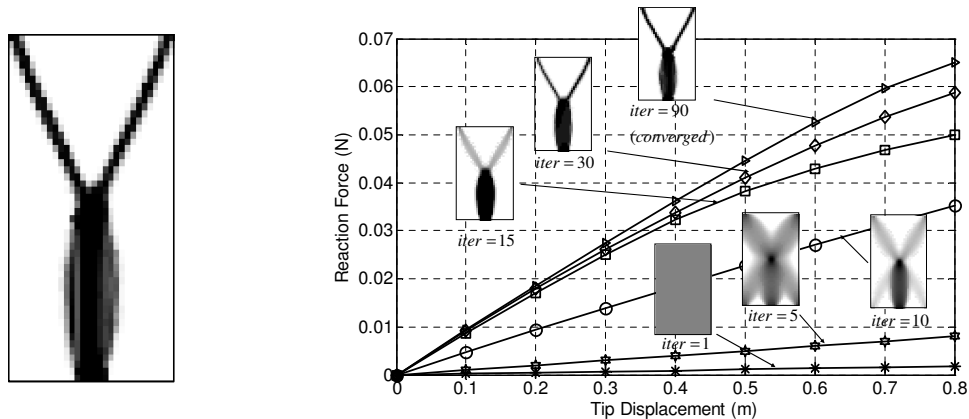


Figure 13. Iteration history of the load-displacement trajectories. The design objective is to find the target layout in Figure 12d.

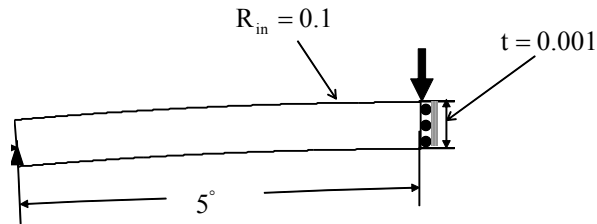


Figure 14. A problem to find a target snap-through trajectory ($E = 1 \text{ N/m}^2$, $\nu = 0.4$, volume = 30%, input displacement = 0.001).

illustrated as the iteration proceeds. The target trajectory in Figure 12a is shown to be accurately traced by the trajectory of the optimized layout in Figure 13. Interestingly, the optimized layout in this case looks like a combination of the two layouts in parts (b) and (c) of Figure 12, with the size of every member roughly reduced by a factor of two. As remarked in earlier examples, it is difficult to obtain a completely distinct solid-void distribution without intermediate design variables.

Example 4: A design exhibiting snap-through. A problem involving snap-through is now considered. Since a relatively simple solver is employed, a structure without any snap-back is considered in Figure 14. The design domain is bounded by elliptical curves. If a slender symmetric structure is center-loaded, the design domain in Figure 14 can be viewed as its half. Then one can consider a roller-supported side which is loaded by a vertical displacement. The left side may be assumed to be fixed at its middle point. The radius and thickness of the ellipse are assumed to be 0.1 and 0.001, respectively. The domain is discretized by 120 by 20 elements and the allowed material usage is set to 30% of the total area. The input displacement is set to be 0.001 which is the same as the height of the design domain. This value would be sufficiently large to induce a snap-through phenomenon. The target points in the load-displacement curve for the topology optimization are marked in Figure 15, right. This curve is so selected as to be able to obtain a layout exhibiting snap-through. To obtain the optimized layout in Figure 15, left, the same ECP formulation as used in the previous examples is used. Solution convergence was stable. The trajectory by the optimized layout is marked by a solid line in Figure 15, right. This example demonstrates that the developed method can be used to solve problems involving snap-through phenomena. However, the present approach in its current form may not handle complex force-displacement curves without an advanced nonlinear solver.

Example 5: A column design exhibiting geometrically weakening. As the last case study, we consider an optimization problem to find a structure tracing the nonlinear load-displacement trajectory given in Figure 16, left. As shown by that figure, the target trajectory corresponds to the load-displacement curve of a slender column vertically loaded at the top left corner. Obviously, the solid straight column will be an optimized layout obtained as a solution to (22) and (23). To set up a nontrivial optimization problem, we take the design problem depicted in Figure 16, right; only the middle part of the column is assumed to be a design domain, but it is enlarged by 5 times. If the mass constraint of 20% is used, then the original straight column (middle diagram) is expected to be recovered. However, the actual optimized result is a rectangular box, quite different from the expected nominal rectangular solid. Seven points in

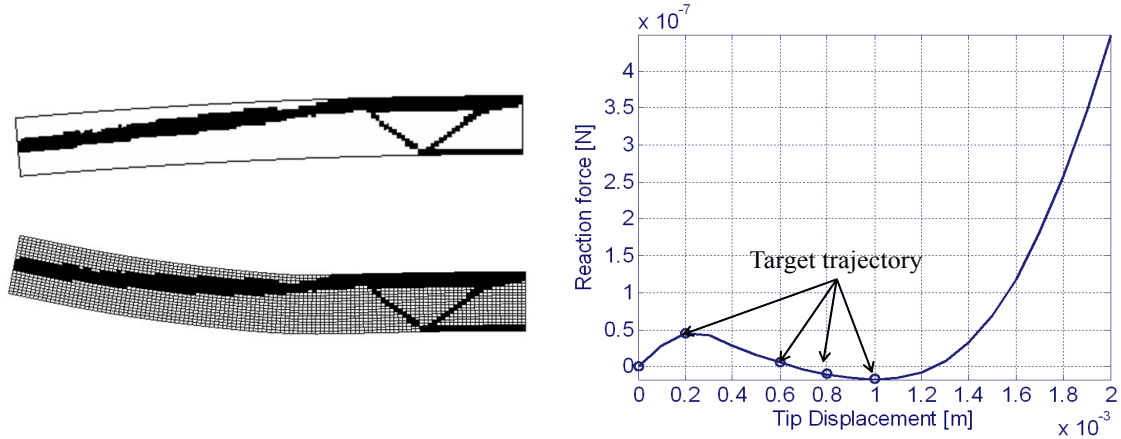


Figure 15. Example 4: a problem involving snap-through. Top left: optimized layout (undeformed). Bottom left: deformed shape (input displacement = 0.001). Right: load-displacement trajectory by the optimized layout; circles represent the target points.

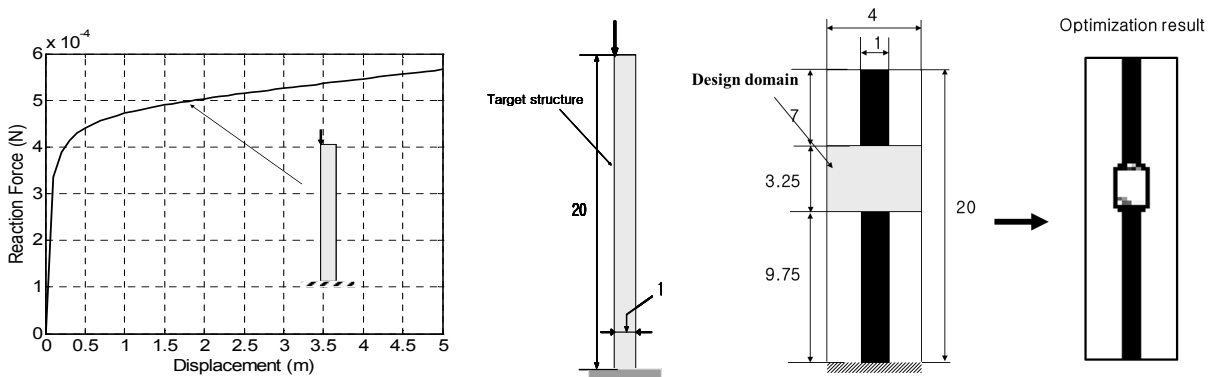


Figure 16. Example 5: a column design exhibiting geometrically weakening. Left: target trajectory. Middle: reference solid column structure ($E = 1 \text{ N/m}^2$, $\nu = 0.3$). Right: an optimized layout in the expanded middle design domain.

the trajectory were used as the reference points to obtain the results in Figure 16, right, by the proposed topology optimization method. When a uniformly distributed density value of 0.2 (corresponding to 20%) was used, the solid column in the middle diagram was not recovered; one of local optima as given by the rightmost diagram was obtained. As Figure 17 shows, however, the optimized layout in Figure 16, right, obtained with 7 reference points, traces fairly closely the target trajectory. Figure 17 also shows the importance of using more reference points in order to trace the target trajectory accurately.

5. Conclusions

The structural topology problem to find optimal structural layouts exhibiting either geometrically hardening or weakening load-displacement trajectories was investigated by using the element connectivity

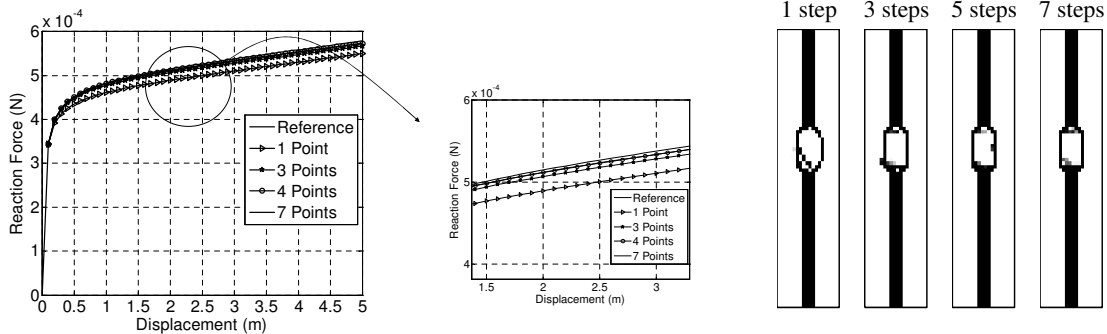


Figure 17. Comparison of the target load-displacement trajectory and the trajectories of the optimized structures obtained with varying numbers of reference points in the load-displacement trajectory. The layouts on the right correspond to, respectively, 1, 3, 4, and 7 points.

parametrization formulation. The following findings are made through this study. First, the ECP method effectively avoided the numerical instability or the erratic convergence related to low-density elements during the topology optimization tracing geometrically nonlinear load-displacement trajectories without any additional stabilization treatment in the Newton–Raphson scheme or prior tuning in optimization. Second, the issues of local optima and gray elements due to the design variable relaxation from the binary variables to the continuous variables appeared in the ECP based method, but the gray element problems appeared to be less severe than those with the element based approach. A load-displacement trajectory sufficiently close to the target one was found while the optimized layout was completely different from the nominal layout used to produce the target trajectory. Therefore, much attention should be paid in interpreting optimized results. In several cases, the postprocessed layouts yielded different load-displacement trajectories from those of the unprocessed layouts. Although a gray-element-free topology optimization formulation that can handle arbitrarily shaped load-displacement curve requires further research, the findings and numerical results obtained with the ECP formulation suggest that it can be very useful to advance the research in complete handling of general nonlinear problems.

Personal notes in memory of MarieLu Steele, by Yoon Young Kim

MarieLu was one of the most cheerful and lively persons I have met. She was always positive, and, I was revitalized every time I was in her company. I strongly believe that her positive energy enabled the dramatic success of the *International Journal of Solids and Structures* for which she was a dedicated Associate Editor for many years. Recently, her enthusiasm and devotion ensured the successful launching of the *Journal of Mechanics of Materials and Structures*, a new high-quality journal in the field of mechanics. I will dearly miss her energizing power and dedication to the mechanics community.

References

- [Bathe 1996] K.-J. Bathe, *Finite element procedures*, Prentice Hall, Englewood Cliffs, NJ, 1996.
 [Bendsøe and Kikuchi 1988] M. P. Bendsøe and N. Kikuchi, *Generating optimal topologies in structural design using a homogenization method*, Matematisk Institut, Danmarks Tekniske Højskole, Lyngby, 1988.

- [Bendsøe and Sigmund 2003] M. P. Bendsøe and O. Sigmund, *Topology optimization: theory, methods and applications*, Springer, Berlin, 2003.
- [Bruns and Sigmund 2004] T. E. Bruns and O. Sigmund, "Toward the topology design of mechanisms that exhibit snap-through behavior", *Comput. Methods Appl. Mech. Eng.* **193**:36-38 (2004), 3973–4000.
- [Bruns and Tortorelli 2003] T. E. Bruns and D. A. Tortorelli, "An element removal and reintroduction strategy for the topology optimization of structures and compliant mechanisms", *Int. J. Numer. Methods Eng.* **57**:10 (2003), 1413–1430.
- [Bruns et al. 2002] T. E. Bruns, O. Sigmund, and D. A. Tortorelli, "Numerical methods for the topology optimization of structures that exhibit snap-through", *Int. J. Numer. Methods Eng.* **55**:10 (2002), 1215–1237.
- [Buhl et al. 2000] T. Buhl, C. B. W. Pedersen, and O. Sigmund, "Stiffness design of geometrically nonlinear structures using topology optimization", *Struct. Multidiscip. Optim.* **19**:2 (2000), 93–104.
- [Cho and Jung 2003] S. Cho and H.-S. Jung, "Design sensitivity analysis and topology optimization of displacement-loaded non-linear structures", *Comput. Methods Appl. Mech. Eng.* **192**:22–24 (2003), 2539–2553.
- [Cook et al. 2001] R. D. Cook et al., *Concepts and applications of finite element analysis*, 4th ed., Wiley, New York, 2001.
- [Hellweg and Crisfield 1998] H.-B. Hellweg and M. A. Crisfield, "A new arc-length method for handling sharp snap-backs", *Comput. Struct.* **66**:5 (1998), 704–709.
- [Huang and Xie 2008] X. Huang and Y. M. Xie, "Topology optimization of nonlinear structures under displacement loading", *Eng. Struct.* **30**:7 (2008), 2057–2068.
- [Kamat and Ruangsilasingha 1985] M. P. Kamat and P. Ruangsilasingha, "Optimization of space trusses against instability using design sensitivity derivatives", *Eng. Optim.* **8**:3 (1985), 177–188.
- [Langelaar et al. 2005] M. Langelaar, G. H. Yoon, Y. Y. Kim, and F. van Keulen, "Topology optimization of shape memory alloy actuators", in *WCSMO6: Proceedings of the 6th World Congress on Structural and Multidisciplinary Optimization* (Rio de Janeiro, 2005), edited by J. Herskovits et al., International Society for Structural and Multidisciplinary Optimization/COPPE, Rio de Janeiro, 2005.
- [Liu and Nocedal 1989] D. C. Liu and J. Nocedal, "On the limited memory BFGS method for large scale optimization", *Math. Program.* **45**:1–3 (1989), 503–528.
- [Lu and Kota 2003] K.-J. Lu and S. Kota, "Synthesis of shape morphing compliant mechanisms using a load path representation method", pp. 337–348 in *Smart structures and materials 2003: Modeling, signal processing, and control* (San Diego, CA, 2003), edited by R. C. Smith, SPIE Proceedings **5049**, SPIE, Bellingham, WA, 2003.
- [Ohsaki 2005] M. Ohsaki, "Design sensitivity analysis and optimization for nonlinear buckling of finite-dimensional elastic conservative structures", *Comput. Methods Appl. Mech. Eng.* **194**:30-33 (2005), 3331–3358.
- [Prasad and Diaz 2006] J. Prasad and A. R. Diaz, "Synthesis of bistable periodic structures using topology optimization and a genetic algorithm", *J. Mech. Des. (ASME)* **128**:6 (2006), 1298–1306.
- [Santer and Pellegrino 2008] M. Santer and S. Pellegrino, "Compliant multistable structural elements", *Int. J. Solids Struct.* **45**:24 (2008), 6190–6204.
- [Saxena 2005] A. Saxena, "Synthesis of compliant mechanisms for path generation using genetic algorithm", *J. Mech. Des. (ASME)* **127**:4 (2005), 745–752.
- [Sekimoto and Noguchi 2001] T. Sekimoto and H. Noguchi, "Homologous topology optimization in large displacement and buckling problems", *JSME Int. J. A Mech. M.* **44**:4 (2001), 616–622.
- [Svanberg 1987] K. Svanberg, "The method of moving asymptotes: a new method for structural optimization", *Int. J. Numer. Methods Eng.* **24**:2 (1987), 359–373.
- [Thai and Kim 2009] H.-T. Thai and S.-E. Kim, "Large deflection inelastic analysis of space trusses using generalized displacement control method", *J. Constr. Steel Res.* **65**:10-11 (2009), 1987–1994.
- [Vila et al. 1997] A. Vila, A. Rodríguez-Ferran, and A. Huerta, "A note on a numerical benchmark test: an axisymmetric shell under ring loads", *Commun. Numer. Methods Eng.* **13**:3 (1997), 181–192.
- [Yoon 2010] G. H. Yoon, "Maximizing the fundamental eigenfrequency of geometrically nonlinear structures by topology optimization based on element connectivity parameterization", *Comput. Struct.* **88**:1–2 (2010), 120–133.

- [Yoon and Kim 2005a] G. H. Yoon and Y. Y. Kim, “Element connectivity parameterization for topology optimization of geometrically nonlinear structures”, *Int. J. Solids Struct.* **42**:7 (2005), 1983–2009.
- [Yoon and Kim 2005b] G. H. Yoon and Y. Y. Kim, “The element connectivity parameterization formulation for the topology design optimization of multiphysics systems”, *Int. J. Numer. Methods Eng.* **64**:12 (2005), 1649–1677.
- [Yoon et al. 2007] G. H. Yoon, J. S. Jensen, and O. Sigmund, “Topology optimization of acoustic-structure interaction problems using a mixed finite element formulation”, *Int. J. Numer. Methods Eng.* **70**:9 (2007), 1049–1075.
- [Yoon et al. 2008] G. H. Yoon, Y. Y. Kim, M. Langelaar, and F. van Keulen, “Theoretical aspects of the internal element connectivity parameterization approach for topology optimization”, *Int. J. Numer. Methods Eng.* **76**:6 (2008), 775–797.

Received 31 Mar 2010. Revised 1 Nov 2010. Accepted 2 Nov 2010.

GIL HO YOON: ghy@hanyang.ac.kr

Department of Mechanical Engineering, Hanyang University, 222 Wangsimni-ro, Seongdong-gu, Seoul 133-791, South Korea

JIN YEE NOH: jyn@knu.ac.kr

School of Mechanical Engineering, Kyungpook National University, South Korea

YOON YOUNG KIM: yykim@snu.ac.kr

Multiscale Design Center and Integrated Design and Analysis of Structures Laboratory, School of Mechanical and Aerospace Engineering, Seoul National University, Kwanak-Gu San 56-1, Seoul 151-742, South Korea